Cancer Letters 326 (2012) 41–51

Contents lists available at SciVerse ScienceDirect

Cancer Letters

journal homepage: www.elsevier.com/locate/canlet

Inhibition of Ca^{2+}-activated Cl^- channel ANO1/TMEM16A expression suppresses tumor growth and invasiveness in human prostate carcinoma

Wen Liu [a], Min Lu [b], Baogang Liu [c], Yi Huang [d,*], KeWei Wang [a,e,*]

[a] Department of Neurobiology, Neuroscience Research Institute, Peking University Health Science Center, China
[b] Department of Pathology, Peking University Health Science Center, China
[c] Department of Pulmonary Oncology, The Third Affiliated Hospital of Harbin Medical University, Harbin 150040, China
[d] Department of Urology, Peking University Third Hospital, China
[e] Department of Molecular and Cellular Pharmacology, Peking University School of Pharmaceutical Sciences, 38 Xueyuan Road, Beijing 100191, China

ARTICLE INFO

Article history:
Received 28 March 2012
Received in revised form 6 July 2012
Accepted 11 July 2012

Keywords:
Prostate cancer
ANO1
PC-3 cells
Proliferation
Metastasis

ABSTRACT

The etiology of prostatic adenocarcinoma remains unclear. Prostate cancer cells of varying metastatic potential and apoptotic resistance show altered expression of plasma membrane ion channels and unbalanced Ca^{2+} homeostasis. Ca^{2+}-activated Cl^- channels (CaCCs) are robustly expressed in epithelial cells and function to regulate epithelial secretion and cell volume for maintenance of ion and tissue homeostasis in proliferation, differentiation and apoptosis. ANO1/TMEM16A was recently identified as a CaCC, and it is of interest to determine whether ANO1 plays a role in development and metastasis of prostate carcinoma. Here we show that ANO1 mRNA and protein are highly expressed in human metastatic prostate cancer LNCaP and PC-3 cells by quantitative analysis of real-time PCR and Western blot. These findings were confirmed by whole-cell patch clamp recording of LNCaP and PC-3 cells with increased current density of ANO1 channels. Immunohistochemistry staining further revealed overexpression of ANO1 in human prostate cancer tissues, which correlated with the clinical TNM stage and Gleason score. Experiments with small hairpin RNAs (shRNAs) targeting human ANO1 resulted in a significant reduction of proliferation, metastasis and invasion of PC-3 cells using WST-8, colony formation, wound-healing and transwell assays. Moreover, intratumoral injection of ANO1 shRNA completely inhibited established tumor growth and survival in orthotopic nude mice implanted with PC-3 cells. Our findings provide compelling evidence that upregulation of CaCC ANO1 is involved in the proliferation, progression and pathogenesis of metastatic prostate cancer. Membrane ANO1 protein may therefore serve as a biomarker, and inhibition of overexpressed ANO1 has potential for use in prostate cancer therapy.

1. Introduction

Prostatic adenocarcinoma arises in the glandular epithelial cells and is one of the most common malignancies in males. However, the pathogenesis of prostate cancer has not been clearly defined [1]. Increasing evidence suggests that Ca^{2+} homeostasis is altered, and upregulated expression of voltage-gated ion channels becomes epigenetically abnormal in metastatic carcinoma cells [2–4]. Ion channels are membrane proteins present in excitable or non-excitable cells, participating in diverse physiological activities integral to excitability, contraction, the cell cycle, salt and water secretion and metastatic cascades [5]. They are crucial for maintaining tissue homeostasis during cellular proliferation, differentiation and apoptosis. The major mechanisms by which ion channels contribute to these crucial events include governing cellular ion fluxes, regulating cell volume and generating membrane potential [6,7].

Chloride channels are important for control of transepithelial transport, regulation of cell volume and membrane excitability. Activation of chloride currents through volume-regulated anion channels (VRACs) in response to cell swelling ($I_{Cl,SWELL}$) is one of the critical mechanisms by which cells restore their volume following osmotic perturbations and stress, a process which is known as regulatory volume decrease (RVD) [8–10]. Effective counteraction of abrupt volume changes, and maintenance of constant cell volume and ion homeostasis during active uptake, exocytosis, proliferation and differentiation are major prerequisites for cell survival [11]. There is evidence that overexpression of antiapoptotic Bcl-2 protein upregulates swelling-activated Ca^{2+} entry that is a critical signal for normal RVD and activation of swelling-activated Cl^- channel activity [12], indicating a causal link between apoptotic resistance and upregulation of swelling-activated Cl^- current and ion flux. In androgen-dependent apoptosis-resistant prostate

* Corresponding authors. Address: Department of Molecular and Cellular Pharmacology, Peking University School of Pharmaceutical Sciences, 38 Xueyuan Road, Beijing 100191, China (K. Wang). Tel./fax: +86 10 82805065.
E-mail addresses: flyinghorse@china.com.cn (Y. Huang), wangkw@bjmu.edu.cn (K. Wang).

0304-3835/$ - see front matter © 2012 Elsevier Ireland Ltd. All rights reserved.
http://dx.doi.org/10.1016/j.canlet.2012.07.015

cancer cells (LNCaP), there is prominent swelling-activated Cl^- current that provides effective RVD under hypoosmotic stress [13,14], implying that Ca^{2+} homeostasis and volume homeostasis of prostate cancer cells are interrelated based on their functional coupling [15].

Calcium-activated chloride channels (CaCCs) are major regulators of epithelial secretion and cell volume regulation [16,17]. TMEM16A (also known as DOG1, ORAOV2, or TAOS-2) was independently demonstrated to be a bona fide Ca^{2+}-activated Cl^- channel (CaCC) [18–20]. It has also been referred to as anoctamin 1 (ANO1) because the channels are ANion selective and have eight (OCT) transmembrane segments [19]. ANO1/TMEM16A is a member of a family with nine other members (known as ANO2-10 or TMEM16B-K) that all share a similar structure with eight putative transmembrane domains and cytosolic amino- and carboxy termini. The *ANO1/TMEM16A* gene is localized on 11q13 [21], and this region of the chromosome is frequently amplified in human cancer [22], and is associated with a poor prognosis. This suggests that a cassette *ANO1/TMEM16A* gene drives 11q13 amplification by providing growth or metastatic advantage to cancer cells [23,24]. ANO1/TMEM16A protein is upregulated in gastrointestinal stromal tumors [25]. The relationship between cancer and channel protein in Ca^{2+}-dependent Cl^- transport is unclear, but raises a question as to whether the chloride channel plays a role in tumorigenesis of prostate epithelial cancer.

In the present study, we found that CaCC ANO1 is highly expressed in human prostate cancer cells (PC-3), where increased current density of ANO1 channels was confirmed by whole-cell patch clamp recordings. In human prostate cancer tissues, the high level expression of ANO1 correlates with the TNM stage and Gleason score. RNA interference-mediated knockdown of ANO1 can inhibit proliferation, metastasis and invasion of prostate cancer cells, and can decrease tumor growth in nude mice implanted with PC-3 cells, suggesting this molecule is a potential biomarker for prostate cancer and a target for antitumor therapy.

2. Materials and methods

2.1. Cell culture and transfection

LNCaP, PC-3 and DU145 cells (human prostate carcinoma cells) were gifts from Dr. Dalong Ma at the Center for Human Disease Genomics, Peking University. Normal RWPE-1 cells (human normal prostate epithelial cells) were purchased from the ATCC (American Type Culture Collection, Rockville, MD). Cells were maintained in complete medium (RPMI 1640 medium) supplemented with 10% fetal calf serum, 100 IU/ml penicillin G, and 100 mg/ml streptomycin under standard culture conditions. After washing, cells were detached with trypsin–EDTA solution and resuspended in fresh medium for subsequent experiments. Transfection with plasmids was carried out using Lipofectamine™ 2000 reagent (Invitrogen, Carlsbad, USA) according to the manufacturer's instructions. Cells with >75% transfection efficiency were used for further experiments. In all experiments with shRNA cell transfection, a shRNA missense plasmid was included as negative control.

2.2. Real time-polymerase chain reaction

Total RNA was extracted from cells with Trizol reagent (Invitrogen). Two micrograms of total RNA were subjected to reverse transcription using an RT-PCR kit (Promega, Madison, USA). Real-time PCR was carried out using the SYBR® Premix Ex TaqTM II kit (TAKARA, Japan). All PCR reactions were performed in a total volume of 20 μl with the following sequence: one cycle of initial denaturation for 30 s at 95 °C and 40 amplification cycles (5 s of denaturation at 95 °C and 34 s of annealing and extension at 60 °C). For real-time PCR, ANO1/TMEM16A and control primers used in this study were as follows: forward primer for ANO1/TMEM16A, TCTGCTGGATGAAGTTTACGG; reverse primer for ANO1/TMEM16A, AGGCGACA TAGAAGATGGGAG; forward primer for β-actin, TGTTACCAACTGGGACGAC and reverse primer for β-actin GGTGTTGAAGGTCTCAAACAT. The threshold cycle (Ct) values obtained from these experiments were used to indicate the fractional cycle numbers at which the amount of amplified target reached a fixed threshold. The amount of ANO1/TMEM16A mRNA in cancer cells, normalized to the internal control (β-actin) and evaluated relative to a calibrator (normal prostate epithelial cells), is given by $2^{-\Delta\Delta Ct}$, where Ct indicates the cycle number at which the fluorescence signal of the PCR product crosses an arbitrary threshold set within the exponential phase of the PCR. $\Delta\Delta Ct = [(Ct_{\text{target (unknown sample)}} - Ct_{\text{end-control (unknown sample)}})] - [(Ct_{\text{target (calibrator sample)}} - Ct_{\text{end-control (calibrator sample)}})]$, which correlates the expression of the gene of interest with the control gene. All PCR reactions were performed with equal amounts of cDNA using the ABI PRISM 7500 Real-Time PCR System.

2.3. Western blot analysis

Cells were washed twice with ice-cold phosphate-buffered saline (PBS) and lysed in RIPA buffer containing 1 X Halt phosphatase and protease inhibitor cocktails (Pierce, Rockford, IL). Cell lysates were centrifuged at 13,000 rpm for 10 min at 4 °C. Protein content in the supernatant was determined with a BCA protein assay kit (Thermo Scientific, USA). Equal amounts of lysate protein (30 μg) were separated on an 8% SDS–PAGE gel, and the proteins were electrophoretically transferred onto nitrocellulose membranes. The blotting membrane was blocked with 5% milk in tris-buffered saline (TBS) buffer for 1 h and incubated overnight at 4 °C with rabbit anti-ANO1/TMEM16A (1:1000; Abcam) and goat anti-β-actin (1:500; Santa Cruz, CA). The membrane was washed with TBS and incubated with anti-rabbit or goat IgG-HRP secondary antibody (1:5000, Santa Cruz, CA). For protein visualization, the nitrocellulose membrane was incubated for 2–3 min using the Immobilon Western HRP Substrate (that contains HRP substrate peroxide Solution and HRP substrate luminal Reagent) prior to exposure of KODAK film. The expression levels of ANO1/TMEM16A and β-actin proteins were quantified with densitometry using Quantity one (Biorad). The signal strength of ANO1/TMEM16A was normalized to the corresponding β-actin control.

2.4. Immunohistochemical staining

An array of normal tissue from multiple human organs was used in this study (US Biomax Inc., catalog No. BN1002). This tissue microarray contained 20 types of normal organs with five specimens per organ, including stomach, brain, colon, bone marrow, rectum, cervix, small intestine, ovary, esophagus, breast, liver, prostate, pancreas, testis, lung, spleen, kidney, lymph node, skin and thymus gland. The human prostate carcinoma tissue array (US Biomax Inc., catalog No. PR8010) included carcinomas ranging from TNM stage I to IV, and all of these samples were from surgical resection specimens from patients of 26–82 years of age. Human pathologic tissue collections which consisted of 10 cases of BPH (Benign prostate hyperplasia) and 17 cases of prostate cancer were obtained from Peking University Third Hospital. Normal human stomach tissue was a gift from the Department of Pathology, Peking University Health Science Center.

Tissue sections were deparaffinized in xylene and hydrated in a graded series of alcohols, followed by incubation with 3% hydrogen peroxide for 10 min at 37 °C. Tissue sections were then placed in 0.01 M citrate antigen retrieval solution (pH 6.0), heated at 95 °C in a microwave oven for 10 min and cooled to room temperature. Slides were washed with PBS and reacted overnight at 4 °C with primary rabbit polyclonal antibody to ANO1 (Ab. dilution 1:100, ab53212, Abcam). PBS and rabbit IgG (dilution 1:5000, ZDR-5002, ZSGB-BIO, China) were used for negative control sections. After slides were washed with PBS, they were incubated with goat anti-rabbit IgG-HRP (PV9000, Zymed Laboratories, South San Francisco, CA) for 30 min at 37 °C, and the reaction was visualized with aminoethylcarbazole (AEC) as a chromogen (Zymed Laboratories, South San Francisco, CA). This AEC chromogen color reaction is red in all sections and photomicrographs. Finally, all sections were counterstained lightly with hematoxylin for 15 s [26].

Tissue specimen/samples were observed with a light microscope (Olympus BX51). The immunohistochemical labeling was assessed by two experienced pathologists in a double blind manner, and the distribution of staining of cancer cells was scored as 0 (less than 25% of cells positive), 1+(25–50% of cell positive), 2+(50–75% of cells positive) and 3+(greater than 75% of cells positive). The staining intensity was scored as negative (0), mild (1+), moderate (2+), and strong (3+).

2.5. Whole-cell patch clamp recordings

Normal human prostate epithelial cells (RWPE-1), and human prostate carcinoma cells (LNCaP, PC-3 and DU145 cells) were seeded on glass coverslips. Whole-cell recordings were performed at room temperature using an EPC-10 patch clamp amplifier in combination with Patchmaster (HEKA). Patch electrodes were pulled from borosilicate glass and filled with an internal solution containing (units in mM) 140 NMDG-Cl, 7.4 Ca^{2+}-EGTA, 2.6 NMDG-EGTA, and 10 NMDG-HEPES. The pipette electrode had a final resistance of 3–5 MΩ. The external solution contained (mM) 140 NMDG-Cl, 5 KCl, 2 CaCl2, 1 MgCl2, and 10 NMDG-HEPES. The pH value of all solutions was adjusted to 7.2 with N-methyl-D-glucamine (NMDG) [20]. The cell was clamped from holding potential (−80 mV) to voltages between −100 and +100 mV in 20 mV steps.

2.6. shRNA preparation and plasmid construction

ANO1/TMEM16A shRNA (short hairpin RNA) and negative control shRNA plasmid were constructed by GeneChem Co., Ltd. (Shanghai, China). There were three sites for siRNA targeting of the human *ANO1/TMEM16A* gene (GenBank

NM_018043): CGTGTACAAAGGCCAAGTA (1077–1095 nt), GCATCTATTTGACTTGTCT (991–1009 nt) and CGAAGAAGATGTACCACAT (837–855 nt). BLAST was performed to ensure that these siRNAs did not have significant sequence homology with other genes. An expression vector containing non-specific siRNA was designed as a negative control. The integrity of expression plasmids was confirmed by DNA sequencing analysis.

2.7. Cell proliferation assays

For assay of cell proliferation, a parallel assay for viability was used with the Cell Counting Kit-8 (Dojindo Laboratories, Japan). The number of viable cells was estimated using the WST-8 assay which provides effective and reproducible determination of proliferative activity [27]. Briefly, WST-8 [2-(2-methoxy-4-nitrophenyl)-3-(4-nitrophenyl)-5-(2,4-disulfophenyl)-2H-tetrazolium, monosodium salt] is reduced by the mitochondrial enzyme NAD-dependent succinate dehydrogenase and produces a colored formazan product which is soluble in the culture medium. The amount of formazan dye generated by the activity of intracellular dehydrogenases is directly proportional to the number of living cells. After transfection with ANO1/TMEM16A shRNA3 or control shRNA, cells were inoculated into 96-well plates at 5000 cells/well. To measure the proliferative activity of cancer cells, 10 μl of the Cell Counting Kit solution were added into each well followed by the incubation of these microplates at 37 °C in 5% CO2/95% air for 5 h before measurement of O.D. values at various time points on days 1, 2, 3 and 4. The number of viable cells was quantified by absorbance measured at 450 nm using a microplate reader (Molecular Devices) with a reference wavelength of 650 nm [28].

2.8. Colony formation assay

PC-3 cells transfected with the ANO1-shRNA3 expression vector or control shRNA vector were plated at 200 cells per 35-mm dish. 800 μg/ml G418 were added after transfection for 48 h, and the medium was changed every 2 days. On day 15, G418-resistant colonies were fixed with 2% PFA/PBS and stained with crystal violet. Colonies with $\geqslant$50 cells were counted [29].

2.9. Wound healing assay

Cell mobility was assessed using a scratch wound assay [29]. After transfection with ANO1/TMEM16A shRNA3 or control shRNA for 3 days, tumor cells were cultured in a 6-well plate until confluent. The cell layer was carefully wounded using a sterile tip and washed twice with fresh serum free media. After incubation with serum free medium for time intervals of 0, 12, 24 or 36 h, the cells were photographed at low magnification (40× amplification). These experiments were carried out in triplicate.

2.10. Cell migration/invasion assay

Tumor cell invasion activity was evaluated in Transwell® cell-culture chambers with polycarbonate filters of 8.0 μm pore size (Corning, Acton, MA, USA), and in BioCoat Matrigel Invasion chambers (BD Biosciences, Bedford, MA, USA) coated with basement membrane matrix [30]. After transfection with ANO1/TMEM16A shRNA3 or control shRNA for three days, tumor cells were starved for 18 h in serum free media containing 0.1%BSA, and 1.5×10^4 of cells in 300 μl of medium were placed in the upper chamber of the Transwell. The tumor cells in the upper chamber were allowed to migrate into the lower chamber containing 10% fetal bovine serum (FBS) medium (600 μl) by incubating for 24 h at 37 °C in a 5% CO_2 atmosphere. Cells in the top well of the upper chamber were removed by wiping them off the top membrane with cotton swabs. The membranes were then fixed with methanol, and stained with DAPI (4′,6-Diamidino-2-phenylindole) for visualization of cell nuclei. The cells which had invaded to the lower surface areas were counted under a microscope (200× magnification) and the cell number was taken to represent invasion activity.

2.11. In vivo tumor growth

Male balb/c nu/nu mice (4–6 weeks old) were purchased from the Department of Laboratory Animal Science of Peking University Health Science Center, and housed five animals per cage in microisolator units under temperature-controlled conditions at 70% humidity with free access to standard rodent chow and water. The animals were quarantined for 1 week prior to their use in the study. Experiments were carried out in accordance with the ethical guidelines of Department of Laboratory Animal Science of Peking University Health Science Center. For tumor implantation, PC-3 cells were seeded in RPMI 1640 medium supplemented with 10% FBS in 10 cm plastic dishes. The cells were then washed three times with 1 × PBS and resuspended in 0.1 ml saline solution. Each mouse was injected with 10^7 cells to form a tumor xenograft. When the tumor volume reached about 80–100 mm^3, the tumor-bearing mice were randomly divided into three experimental groups ($n = 4$ mice/group): (1) Blank; (2) control shRNA; and 3) ANO1 shRNA3. ANO1 shRNA3 or control shRNA diluted in saline was directly injected into the tumor xenograft at a dose of 50 μg every week. Tumor volumes were assessed once every week for a total period of 6 weeks by measuring two perpendicular dimensions with a caliper according to the formula volume = $(a \times b^2)/2$, where a is the largest and b is the smallest dimension of the tumor [31].

2.12. Statistical analysis

The data were obtained and statistically analyzed with paired and unpaired t-tests or with the ANOVA test. For analysis of human tissue arrays and human pathologic tissue collections, statistical analysis was performed using the two-tailed Fisher's exact test, and a 2-sided P value of <0.05 was considered statistically significant. Data are presented as mean ± s.e.m. Statistical significance is given as $^{*}p < 0.05$; $^{**}p < 0.01$ and $^{***}p < 0.001$.

3. Results

3.1. ANO1 expression in human normal tissues

In order to investigate the expression level of ANO1 in human normal tissues, we used multiple normal organ human tissue array containing 20 types of normal organs, including stomach, brain, colon, bone marrow, rectum, cervix, small intestine, ovary, esophagus, breast, liver, prostate, pancreas, testis, lung, spleen, kidney, lymph node, skin and thymus gland. Immunohistochemical staining of this array with ANO1 antibody revealed that ANO1 is expressed in human normal stomach, colon, rectum, small intestine, esophagus, liver, pancreas, testis, lung and kidney (Table 1).

3.2. Upregulation of CaCC ANO1 expression in prostate cancer cells

To investigate the expression level of ANO1 in prostate cancer epithelial cells, we began by designing a specific cDNA probe for targeting the N-terminus of ANO1, and selected three classic cell lines of human prostate cancer, LNCaP, PC-3 and DU145. PC-3 cells have high metastatic potential compared to DU145 cells, which have moderate metastatic potential [32]. Quantitative analysis of ANO1 mRNA by real time-PCR showed an increase of about 250% in ANO1 mRNA in PC-3 cells and an increase of about 240% in LNCaP cells, but not in DU145 cells, as compared with normal prostate epithelial cells (RWPE-1), indicating that ANO1 transcripts were upregulated in LNCaP and PC-3 (Fig. 1A). To quantify the relative expression of ANO1 protein, we performed Western blot analysis. ANO1 proteins extracted from LNCaP, PC-3 or DU145 cells were separated by gel electrophoresis under denaturing conditions and probed with ANO1 antibody which specifically recognizes the channel proteins. Fig. 1B shows that the protein level of ANO1 in DU145, LNCaP and PC-3 cells increased 1.24-fold, 2.95-fold and 5.27-fold respectively, as compared with ANO1 protein in normal control cells (RWPE-1). This result is consistent with the quantitative real-time PCR analysis, indicating that ANO1 is upregulated in prostate cancer LNCaP and PC-3 cells.

To further confirm the functional expression of ANO1 channels in prostate cancer cells, we performed whole-cell patch clamp recordings of DU145, LNCaP and PC-3 cells. In response to voltage steps of stimuli, a family of ANO1 currents was recorded in control RWPE-1 cells, and in DU145, LNCaP and PC-3 cancer cells (Fig. 2). The ANO1 current was blocked by the chloride channel blocker DIDS (5 μM). These results show that ANO1 current density was 5.1-fold (3.05 ± 1.2 nA, $n = 9$) in PC-3 cells and 3.9-fold (2.31 ± 0.27 nA, $n = 5$) in LNCaP cells as compared with ANO1 current in RWPE-1 cells (594.8 ± 92.5 pA, $n = 5$). The ANO1 current in DU145 cells (917.5 ± 94 pA, $n = 5$) was slightly higher than that of the RWPE-1 group (Fig. 2B). This demonstrated that functional expression of ANO1 was also upregulated in LNCaP and PC-3 prostate cancer epithelial cells.

Table 1
Tissue distribution of ANO1/TMEM16A in human multiple organs.

Distribution	Total no. of samples	No. of ANO1 positive samples	% Positive (No./total)
Normal gastric tissue	10	10	100
Normal prostate tissue	12	0	0
Normal cerebral tissue	5	0	0
Normal colonic tissue	5	5	100
Normal myeloid tissue	5	5	100
Cancer adjacent normal rectal tissue	5	2	40
Normal uterine cervical tissue	5	5	100
Normal small intestine tissue	5	5	100
Normal ovarial tissue	5	0	0
Normal esophageal tissue	5	5	100
Cancer adjacent normal breast tissue	7	2	28.6
Normal hepatic tissue	5	4	80
Normal pancreatic tissue	5	5	100
Cancer adjacent normal testicular tissue	5	4	80
Normal pulmonary bronchioles	5	5	100
Normal splenic tissue	5	0	0
Normal renal tissue	5	5	100
Normal thymus gland tissue	5	0	0

Note: Immunohistochemical staining with ANO1 antibody reveals ANO1 expression in tissues of stomach, colon, rectum, small intestine, esophagus, liver, pancreas, testis, lung and kidney.

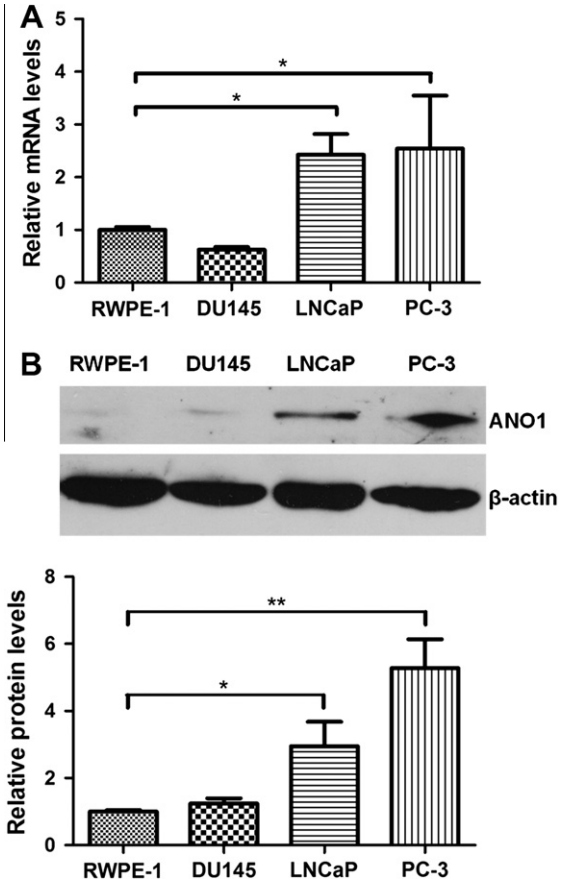

Fig. 1. Up-regulation of ANO1 expression in prostate cancer cells. (A) Quantitative real-time PCR analysis of ANO1 mRNA levels in normal prostate epithelial cells (RWPE-1) and prostate cancer cell lines (DU145, LNCaP and PC-3). The ANO1 mRNA level was increased 2.5-fold in PC-3 and 2.4-fold in LNCaP cells, as compared with that of normal prostate RWPE-1epithelial cells or DU145 cells. (B) Top panel, Western blot analysis of ANO1 protein expression in RWPE-1 cells and in DU145, LNCaP and PC-3 cells by Western blot. The expression of ANO1 protein was normalized to the expression level of β-actin. Bottom panel, the bar graph summary from the top panel shows the relative expression of ANO1 protein in DU145, LNCaP, and PC-3 cells, as compared with RWPE-1. The statistical significance between groups is indicated as, $^{**}p < 0.01$ ($n = 4$). All data are shown as mean ± s.e.m.

3.3. Over expression of ANO1 channel protein in human prostate cancer tissues

To further validate the role of ANO1 in prostate cancer, we examined ANO1 expression in both human pathologic tissue specimens from prostate cancer patients and human tissue arrays by immunohistochemical staining with specific antibody against ANO1. Fig. 3 shows that ANO1 is highly expressed in prostate cancer tissues, as compared with benign prostate hyperplasia (BPH) and benign glands adjacent to carcinoma.

Based on tissue arrays, ANO1 expression was observed in 90.3% of the cases (65/72) and the immunohistochemical scoring for all tissues from prostate cancer patients is shown in Table 2. Based on TNM staging (Tumor, Lymph Nodes, Metastasis), we classified prostate cancer cases into two subgroups consisting of Group 1 containing stage I and II cases, and Group 2 containing stage III and IV cases (Table 3). In Group 1, 88.1% of tumors (37/42) showed negative or weak expression of ANO1, and 11.9% (5/42) of tumors showed strong ANO1 staining (Table 3). In Group 2, 26.6% of tumors (8/30) showed negative or weak expression, whereas 73.4% of tumors (22/30) showed strong ANO1 expression (Table 3). The significant difference between these two groups indicates that higher TNM stage correlates with increased ANO1 expression.

Using the Gleason scoring system that is based on microscopic tumor patterns, we classified the tissues specimen into three subgroups: subgroup 1 (Gleason score <4) where 100% of tumors (3/3) showed negative or weak expression, and on tumor (0/3) showed strong ANO1 expression; subgroup 2 (Gleason score 4–7) in which 71.1% (27/38) of tumors showed negative or weak expression, and 28.9% (11/38) of tumors showed strong expression; and subgroup 3 (Gleason score >7 group) where 51.8% (14/27) of tumors showed negative or weak expression, and 48.2% (13/27) of tumors showed strong ANO1 expression. These results show that higher Gleason scores are associated with greater ANO1 expression.

To further confirm the results obtained from evaluation of tissue arrays, we examined the pathologic tissue specimens from 17 prostate cancer patients. ANO1 expression was observed in 76.5% of cases of carcinoma (13/17) as shown in Table 4A. Using Gleason scoring, we classified the tissues specimen into two subgroups: subgroup 1 (Gleason score 6–7) in which 71.4% (5/7) of tumors showed negative or weak expression, and 28.6% (2/7) of tumors showing strong ANO1 expression; and subgroup 2 (Gleason score >7) where 30% (3/10) of tumors showed negative or weak

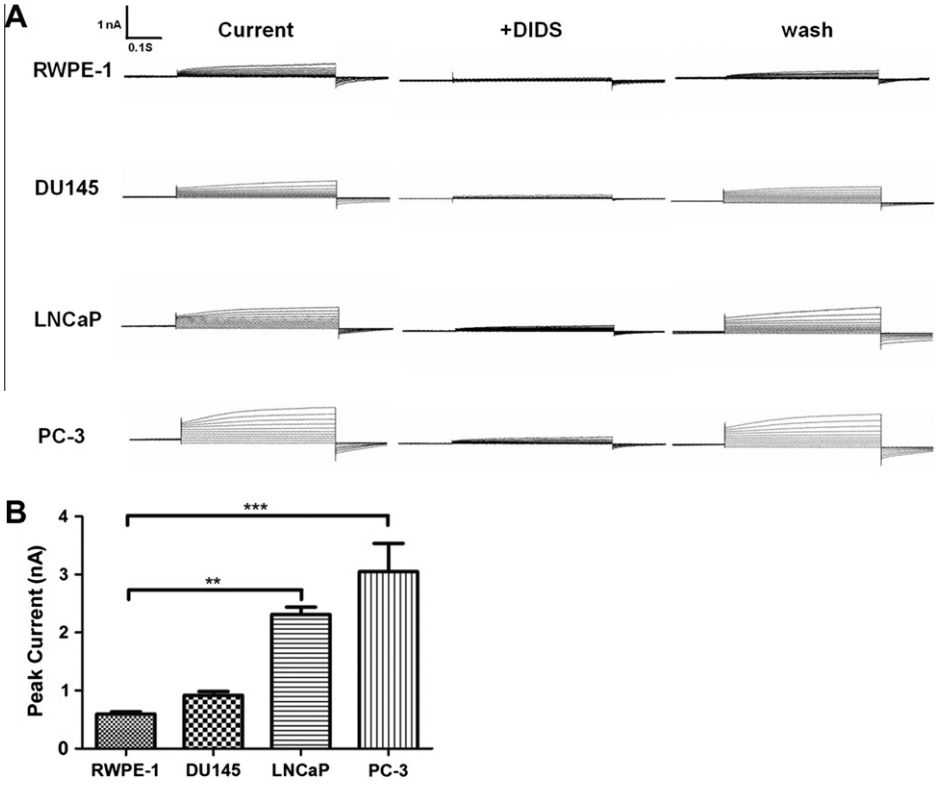

Fig. 2. Functional expression of ANO1 current in prostate cancer cells. (A) Whole-cell ANO1 currents were recorded by whole-cell patch clamp recording and cells were held at −80 mV followed by a family of voltage steps of 20 mV each between −100 and 100 mV. In the presence of CaCC ANO1 blocker DIDS (5 μM) ANO1 current was blocked. Upon washing out, the ANO1 currents were recovered. (B) The bar graph summarizes the peak currents recorded at 100 mV voltage in cancer cells DU145 ($n = 5$), LNCaP ($n = 5$) and PC-3 ($n = 9$), compared with normal control RWPE-1 cells ($n = 5$). Functional expression of ANO1 in PC-3 cells ($n = 9$) was 5.1-fold higher and 3.9-fold higher in LNCaP cells ($n = 5$) than in RWPE-1 cells ($n = 5$), student-t test $^{***}p < 0.001$. All data are shown as mean ± s.e.m.

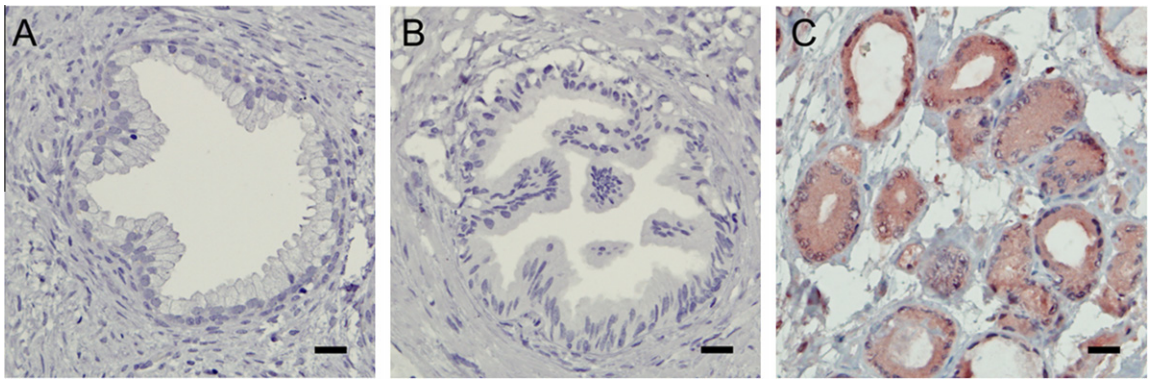

Fig. 3. Immunohistochemical staining of ANO1 expression in human prostate tissues of benign prostate hyperplasia, benign glands adjacent to carcinoma and prostate cancer. (A) Benign prostate hyperplasia (BPH) tissue shows negative staining for ANO1. (B) Benign glands adjacent to carcinoma showing negative ANO1 staining. (C) Representative field showing human prostate cancer tissue with ANO1 staining of neoplastic epithelium. (B and C) are from the same patient. The scale bar indicates 20 μm.

Table 2
ANO1 staining and scoring in human tissue array.

	Total no. of samples	No. of ANO1 positive samples	% Positive (No./total)	*P* value
Normal prostate tissue	5	0	0	
Benign prostate hyperplasia	16	2	12.5	<0.005*
Adenocarcinoma	72	65	90.3	

Note: Tissue specimen from 72 prostate cancer patients and 16 patients with benign prostate hyperplasia, and 5 specimen of normal tissues from cancer-free prostates were analyzed. Positive ANO1staining was seen in 90.3% of patient samples examined.

* Statistical difference in the percentage of ANO1 positive samples between normal tissues or benign prostate hyperplasia and prostate adenocarcinomas ($p < 0.005$)

Table 3
Correlation between ANO1 expression and prostate cancer from human tissue array.

Characteristics		No. of patients	No. of samples in categories of scores for ANO1 immunostaining signal		*P* value
			[0,3]	[4,6]	
Age (y)	>60 y	61	39 (63.9%)	22 (36.1%)	0.736
	⩽60 y	11	6 (54.5%)	5 (45.4%)	
TNM stage	I and II	42	37 (88.1%)	5 (11.9%)	<0.05[a]
	III and IV	30	8 (26.6%)	22 (73.4%)	
Gleason score	<4	3	3 (100%)	0 (0%)	<0.05[b]
	[4,7]	38	27 (71.1%)	11 (28.9%)	
	>7	27	14 (51.8%)	13 (48.2%)	

Note: In the pathologic TNM staging, the stage I and II as a group, and the TNM stage III and IV as a group. There was a significant difference between the two groups, showing the higher the TNM stage the more ANO1 expression. With the Gleason score, there was also significant difference between the three groups, indicating the correlation between prostate cancer and ANO1 expression.

[a] Statistical significance in ANO1 expression between the TNM staging I-II group and the TNM staging III-IV group ($p < 0.05$).

[b] Statistical significance in ANO1 expression among groups of Gleason score less than 4, 4-7 and greater than 7 ($p < 0.05$).

Table 4A
ANO1 staining and scoring in tissues from human pathological tissue specimen.

	Total No. of samples	No. of ANO1 positive samples	% Positive (No./total)	*P* value
Benign prostate hyperplasia	10	0	0	<0.005[*]
Adenocarcinoma	17	13	76.5	

Note: Tissue specimen from 17 prostate cancer patients and 10 patients with benign prostate hyperplasia were analyzed. Positive ANO1 staining was seen in 76.5% of patient samples examined.

[*] Statistical significance in percentage of ANO1 positive samples between benign prostate hyperplasia and prostate adenocarcinomas ($p < 0.005$)

Table 4B
Correlation between ANO1 expression and prostate cancer from human pathological tissue specimen.

Characteristics		No. of patients	No. of samples in categories of scores for ANO1 immunostaining signal		*P* value
			[0,3]	[4,6]	
Age (y)	>60 y	15	7(46.7%)	8(53.3%)	0.735
	⩽60 y	2	1(50%)	1(50%)	
Gleason score	[6,7]	7	5(71.4%)	2(28.6%)	<0.05[a]
	>7	10	3(30%)	7(70%)	

Note: In Gleason score, score 6–7 as a group, and score above 7 as a group. There was a significant difference between these three groups, suggesting that the higher the Gleason score, the more ANO1 expression.

[a] Statistical significance in ANO1 expression between Gleason score 6-7 group and the score >7 group ($p < 0.05$).

expression, and 70% (7/10) of tumors showed strong ANO1 expression (Table 4B). These results further confirmed the positive correlation of ANO1 expression with tumor grade in prostate cancer.

3.4. Inhibition of PC-3 cell proliferation by silencing endogenous ANO1

To investigate the function of ANO1 in proliferation of PC-3 cells, we first designed three short hairpin RNAs (shRNA1-3) targeting the N-terminus of ANO1, and used these probes for *in vitro* silencing of ANO1 gene expression via RNA interference. Transfection of three shRNA1-3 (shRNA1, shRNA2 or shRNA3) in PC-3 cells expressing ANO1 proteins resulted in an 85% reduction in ANO1 expression in the group treated with shRNA1, an 87% reduction with shRNA2, and a 96% reduction with shRNA3, as compared with the control shRNA or positive control (ANO1) in which robust expression of ANO1 remained unaltered (Fig. 4). This confirmed that ANO1 shRNA1 is effective in silencing ANO1 expression, and the ANO1 shRNA3 probe was most effective in silencing endogenous expression of ANO1.

To further examine the role of ANO1 in prostate cancer cell proliferation, we used this ANO1 shRNA3 probe and investigated the effect of shRNA3 on proliferation in PC-3 cells. Cell proliferation was evaluated using the WST-8 assay which is more stable and less cytotoxic than the conventional MTT assay. As shown in Fig. 5A from four independent repetitions of these experiments, transfection of ANO1 shRNA3 resulted in a significant inhibition of PC-3 cell proliferation from 82% on day 2% to 73% on day 3, and 59% on day 4 in a time-dependent manner, as compared with PC-3 cells treated with control shRNA. To further confirm these results, we utilized the Colony Formation assay. As shown in Fig. 5B, transfection of ANO1 shRNA3 resulted in a significant inhibition of PC-3 cell colony formation. These results indicate that silencing endogenous ANO1/TMEM16A can decrease proliferation of prostate cancer PC-3 cells.

3.5. Silencing endogenous ANO1 decreases migration and invasiveness in PC-3 cells

To study the effect of endogenous ANO1 on cell migration, we carried out a scratch wound-healing assay that evaluates wound closure at various time points of the experiment. After transfection of ANO1 shRNA3 or control shRNA for 3 days, tumor cells were cultured until confluent. The cell layer was carefully wounded using sterile tips. ANO1 shRNA3 delayed wound filling of PC-3 cells as compared with control shRNA-treated cells where wound filling was much faster (Fig. 6A), indicating that endogenous ANO1 promotes tumor cell migration.

The most threatening feature of malignancy in cancer is the potential for invasion and metastases. To investigate the role of ANO1 in cell invasion, we examined the effect of ANO1 knockdown on the

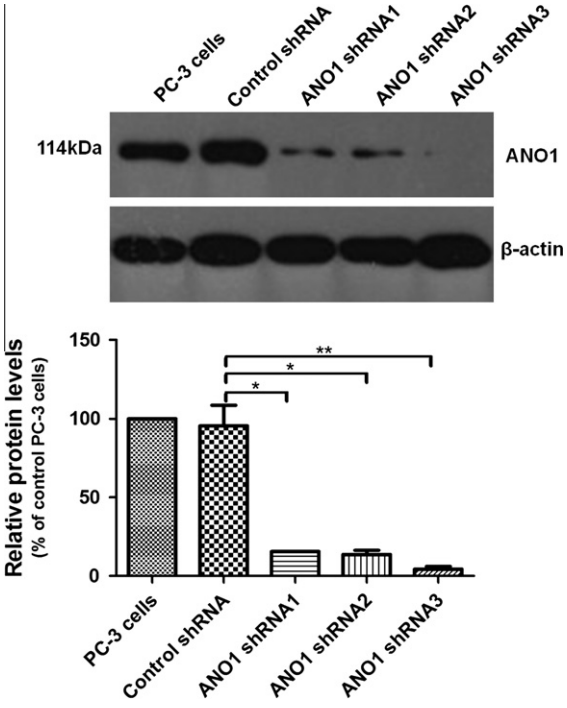

Fig. 4. RNAi knockdown of ANO1 protein expression in PC-3 cells expressing ANO1 proteins. Three different ANO1 shRNAs (shRNA1, shRNA2 and shRNA3) were transfected into ANO1 expressing PC-3 cells. Three days after the transfection, extracted membrane proteins were immunoblotted with ANO1 antibody. Expression of ANO1 protein was normalized with the expression level of β-actin. ANO1 shRNA3 was most effective in silencing ANO1 expression, compared with the other two shRNAs and the control shRNA. The bottom panel summarizes the protein expression of ANO1 from the top panel.

invasive potential of PC-3 cells using the Transwell assay which is used to characterize tumor cell metastasis and progression. After transfection with ANO1 shRNA3 or control shRNA for 3 days, PC-3 cells were starved for 18 h prior to placement in the upper chamber of the Transwell. Cells in the top well were removed by wiping off the top of membrane with cotton swabs. Fig. 6B shows DAPI stained images of PC-3 cells transfected with ANO1 shRNA3 in which the invading cells are significantly fewer than those in the control shRNA group. These results indicate that silencing endogenous ANO1 can decrease migration and invasion in prostate cancer PC-3 cells.

3.6. Suppression of xenograft tumor growth in vivo by ANO1 knockdown

To investigate the effect of ANO1 knockdown on the growth of prostate cancer *in vivo*, 10^7 PC-3 cells were injected into the right flank of mice for formation of a tumor xenograft. When tumor size reached approximately 80–100mm^3, the mice were randomly divided into three groups. ANO1 shRNA3 or control shRNA diluted in saline was directly injected into the tumor xenograft at a dose of 50 μg every week for a continuous period of 6 weeks. Tumor volumes were measured every week during the period of treatment until the animals were sacrificed. During the experiment, no animal death or signs of toxicity were observed. As shown in Fig. 7A and B, the PC-3 cell induced average tumor volume at the termination of the experiment was 782.75 ± 60.72 mm^3 (n = 5) and 868.25 ± 127.32 mm^3 (n = 5) for the blank control and control shRNA respectively. In contrast, treatment with ANO1 shRNA3 resulted in a significant reduction in tumor volume to 224.75 ± 68.37 mm^3 (n = 5), which is about one forth the tumor volume of the control group (Fig. 7B). The average weight of tumor in the ANO1 shRNA group

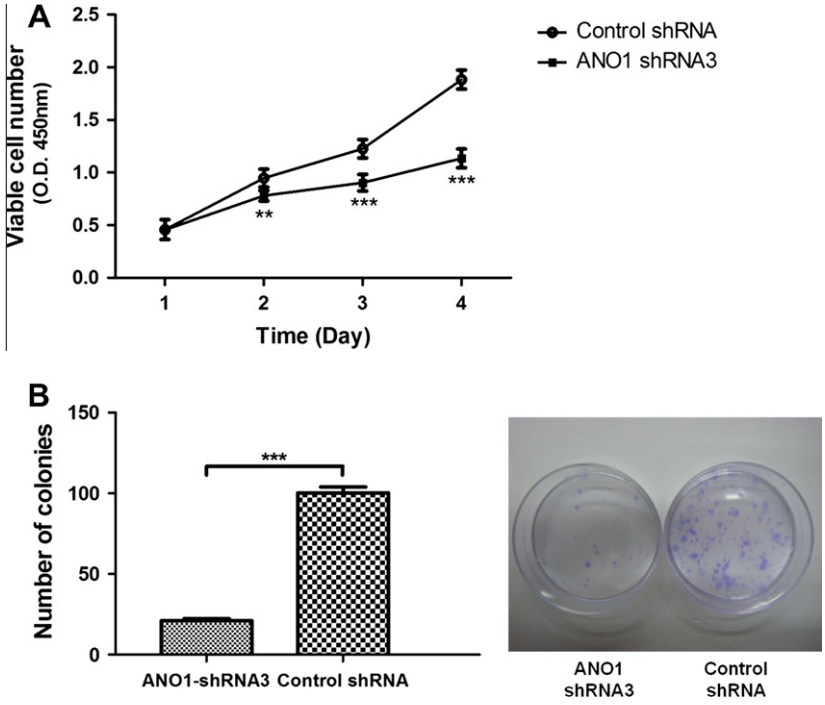

Fig. 5. Suppression of prostate cancer cell proliferation by ANO1 silencing. (A) Cell proliferation of PC-3 cells was first assessed using the WST-8 assay based on the extracellular reduction of WST-8 by NADH produced in the mitochondria (see methods). One day after transfection, the number of PC-3 cells was quantified by the measurement of absorbance at 450 nm using a microplate reader. Transfection of ANO1 shRNA3 resulted in significant inhibition of PC-3 cell proliferation in a time-dependent manner, compared with PC-3 cells treated with control shRNA. The data are presented from four independent repetitions of these experiments. (B) RNAi of ANO1 inhibits the clonogenicity of carcinoma cells (n = 9). Representative inhibition of colony formation by ANO1-shRNA on PC-3 cells. (C) Quantitative analysis of colony numbers. The statistical significance between groups is indicated as, $^{*}p < 0.05$; $^{**}p < 0.01$; $^{***}p < 0.001$ (n = 6). All data are shown as mean ± s.e.m.

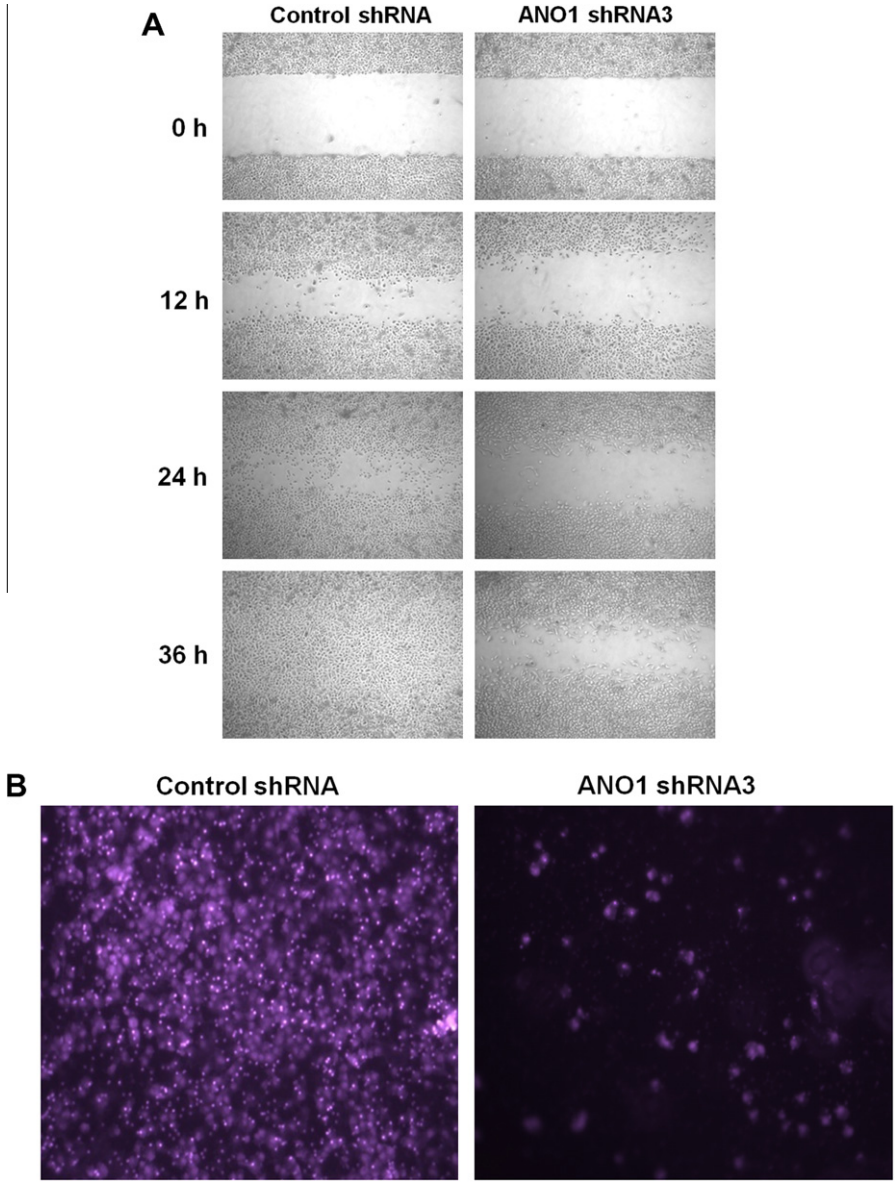

Fig. 6. Inhibition of cell migration and invasion by ANO1 knockdown. (A) PC-3 cell migration was assessed by the wound healing assay in the presence of ANO1 shRNA3, compared with control shRNA. After transfection with ANO1 shRNA3 or control shRNA for 3 days, PC-3 tumor cells were cultured in a 6-well plates until confluent. The cell layer was carefully wounded using sterile tips. During incubation with serum free medium, the wounded cell layer transfected were photographed at time points 0, 12, 24 and 36 h under low magnification (40× magnification). (B) After transfection with ANO1 shRNA or negative control shRNA for 3 days, PC-3 cells were starved for 18 h before cell invasion assays were performed using Matrigel transwell filters. The invading cells were fixed with methanol and stained with DAPI. The image on the left represents one microscopic field of the ANO1 shRNA3 group with decreased cell migration and invasion of PC-3 cells, and the right hand image shows the control shRNA group.

was significantly less (0.49 ± 0.1 g; $n = 4$), as compared with the blank group (1.58 ± 0.22 g, $n = 4$) and control shRNA group (1.62 ± 0.18 g, $n = 4$) (Fig. 7B). H&E stained sections of tumor xenografts showed tumor development in the blank, control shRNA and ANO1 shRNA groups (Fig. 7C), and this was further confirmed by immunohistochemical staining of ANO1 in tumor xenographs (Fig. 7D). These results indicate that knockdown of ANO1 not only suppresses the migration and invasion of prostate cancer cells but also significantly inhibits tumor growth.

4. Discussion

In this study, we have shown for the first time that Ca^{2+}-activated Cl^- channel ANO1/TMEM16A is upregulated in both human prostate epithelial cancer cells and carcinoma tissue samples, and overexpression of ANO1 correlates with TNM stage and Gleason score. The inhibition of ANO1 suppresses tumor cell proliferation and migration *in vitro*, and tumor growth *in vivo*. Our findings have several implications. First, since the ANO1 gene is overexpressed in prostate carcinoma cells, ANO1 proteins may serve as a potential biomarker for diagnosis and prognosis in prostate cancer. Second, perturbed intracellular Ca^{2+} and Cl^- ions and cell volume are critical factors that are likely associated with the pathogenesis, invasiveness and metastatic potential in androgen-independent prostate cancer pathogenesis. Third, *in vitro* and *in vivo* experiments indicate that ANO1 may be a potential therapeutic target for prostate cancer. Development of small molecules aimed at specifically inhibiting ANO1 may prove to be useful in pharmacological intervention in prostate cancer or others carcinomas where ANO1 is overexpressed.

From the analysis of ANO1 expression, we found significant upregulation of ANO1 in prostate carcinoma PC-3 cell lines, but

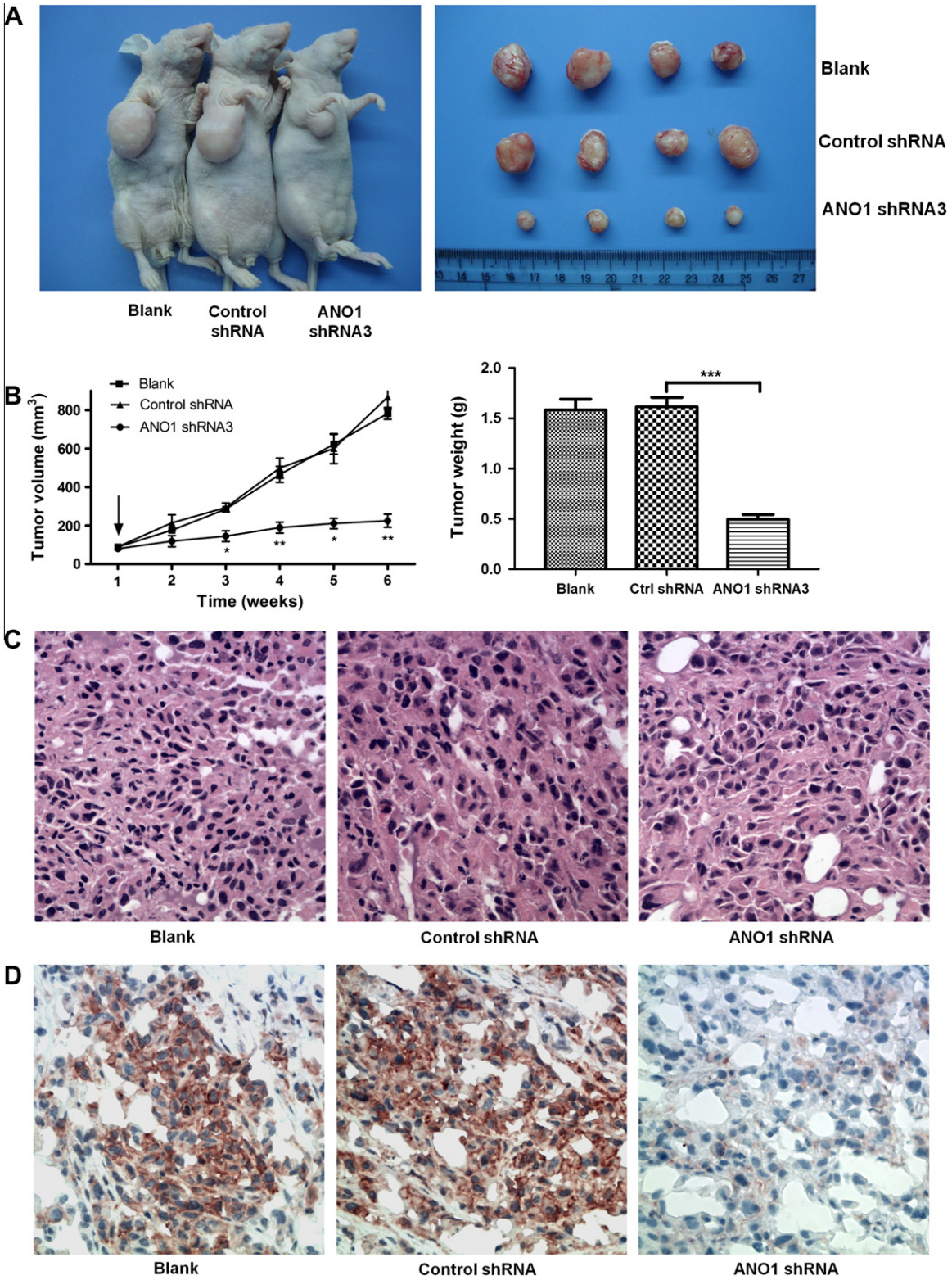

Fig. 7. *In vivo* suppression of tumor cell growth by intratumoral injection of ANO1 shRNA. 10^7 PC-3 cells were injected into the flank of nude mice for formation of a tumor xenograft. ANO1 shRNA3 or control shRNA at a dose of 50 μg was injected into the tumor xenograft after it reached a size of approximately 80–100 mm^3 for 6 consecutive weeks. The tumor size was measured once a week, and tumor growth curves were generated over the 6-week period. (A) Representative images of mice bearing the tumors (top panel) after PC-3 injection; and tumors (bottom panel) on the 42nd day of generation. (B) Measurements of tumor volumes and weights from nude mice at various time points during shRNA treatment. The tumor volumes in each group ($n = 5$) were measured with calipers every 7 days. Statistical significance between groups is indicated as, $^{*}p < 0.05$, $^{**}p < 0.01$, $^{***}p < 0.001$. Data are expressed as mean ± s.e.m. ($n = 5$). (C) Representative H&E staining of tumor xenographs in the blank, control shRNA and ANO1 shRNA groups. (D) Representative immunohistochemical staining of ANO1 in tumor xenographs in blank, control shRNA and ANO1 shRNA groups.

not in DU145 cells. The underlying cause for this difference is not clear, although both PC-3 and DU145 cell lines have both been reported to be androgen receptor-negative or androgen- non-responsive [33–35]. PC-3 cells were originally derived from advanced

androgen-independent prostate cancer bone metastases with high metastatic potential. In contrast, DU145 cells have only moderate metastatic potential [32]. PC-3 cells have low testosterone-5-alpha reductase activity and express prostate specific antigen (PSA) that is produced almost exclusively by cells of the prostate gland. In contrast, DU145 cells were derived from brain metastasis, and they are not hormone sensitive and do not express PSA. However, we cannot exclude the possibility that differences in passage number account for the difference in these two cells lines, although DU145 cells can be passaged *in vitro* for a period of over two years without significant changes in cell organelle structure [36].

Chloride channels are relatively unexplored in tumorgenesis, although ion channels have been shown to play an important role in tumor development, growth and malignancy [37]. In this study, we utilized three different shRNAs that specifically target ANO1 transcripts and this resulted in a significant reduction of ANO1 channel expression and suppression of cell proliferation, migration and invasion. Our results indicate that overexpression of CaCC ANO1 likely makes a direct contribution to prostate cancer tumorgenesis. Homeostasis of cell volume serves to maintain structural integrity and constancy of the intracellular milieu. Maintenance of consistent volume is one of the most critical factors for cellular homeostasis and survival. One of the critical functions of CaCCs is to mediate fluid secretion, which is important in cellular compensatory responses to changes in volume and osmotic stress. Activation of calcium sensitive and voltage-dependent ANO1 as a result of elevation of intracellular calcium is likely to alter the cell volume of cancer cells [38,39]. It has been shown that antiapoptotic oncoprotein BCL-2 regulates cell volume and ion flux by activating swelling-activated Ca^{2+} entry that is critical for normal regulatory volume decrease (RVD) [12]. BCL-2 is also associated with the development of androgen-independent prostate cancer due to its high levels of expression in androgen-independent tumors of advanced stage, suggesting that overexpression of ANO1 in prostate cancer cells most likely induces the overexpression of BCL-2 which in turn results in apoptotic resistance [40,41]. However, further experimental work will be required to test this possibility.

In prostate carcinoma cells, as in other nonexcitable cell types, Ca^{2+} entry from the extracellular space is mainly supported by the capacitative calcium entry (CCE) mechanism for maintenance of Ca^{2+} homeostasis [4,42]. This mechanism is mediated by specialized plasma membrane store-operated Ca^{2+} release-activated channels (CRACs) [43].

CaCC ANO1 is located on chromosome 11 band q13 which seems to be one of the most frequently amplified regions in human cancer and is associated with a poor prognosis [22,23], and as such ANO1 may be of clinical values as a biomarker for diagnosis of prostate cancer and other cancers in which the 11q13 locus is amplified.

In summary, our observations lead to identification of CaCC ANO1/TMEM16A mRNA and protein upregulation in human prostate carcinoma PC-3 cells, and ANO1 was found to be highly expressed in human prostate cancer tissues. Electrophysiology results showed that functional expression of ANO1 in PC-3 cells was much higher than in RWPE-1 cells. More significantly, inhibition of ANO1 expression can suppress proliferation, metastasis and invasiveness *in vitro* and tumor growth *in vivo*. Development of small molecules aimed at specifically inhibiting ANO1 may prove to be useful in pharmacological intervention in prostate carcinoma or other carcinomas where ANO1 is upregulated.

Acknowledgments

We are grateful to Dr. Uhtaek Oh for providing us the ANO1 plasmid construct. We also would like to thank our laboratory members Dr. Xiling Bian and Mr. Yiquan Tang for discussion this research, and Dr. Wenling Han for her help with and comments on this work. We are very grateful to Dr. Mike McNutt for his careful proof-reading of this manuscript. KWW wishes to thank Jingmei Wang for her consistent support during this research. This work was supported by research grants to KWW from the National Science Foundation of China, 30970919 and from the Ministry of Science Technology of China, 2009ZX09301-010 and from the Ministry of Education of China, 111 Project China (B07001).

References

[1] S.M. Edwards, D.G.R. Evans, Q. Hope, A.R. Norman, Y. Barbachano, S. Bullock, Z. Kote-Jarai, J. Meitz, A. Falconer, P. Osin, C. Fisher, M. Guy, S.G. Jhavar, A.L. Hall, L.T. O'Brien, B.N. Gehr-Swain, R.A. Wilkinson, M.S. Forrest, D.P. Dearnaley, A.T. Ardern-Jones, E.C. Page, D.F. Easton, R.A. Eeles, U.G.P.C. Study, Prostate cancer in BRCA2 germline mutation carriers is associated with poorer prognosis, Br. J. Cancer 103 (2010) 918–924.
[2] J.K. Diss, D. Stewart, F. Pani, C.S. Foster, M.M. Walker, A. Patel, M.B. Djamgoz, A potential novel marker for human prostate cancer: voltage-gated sodium channel expression in vivo, Prostate Cancer Prostatic. Dis. 8 (2005) 266–273.
[3] S.P. Fraser, J.K. Diss, A.M. Chioni, M.E. Mycielska, H. Pan, R.F. Yamaci, F. Pani, Z. Siwy, M. Krasowska, Z. Grzywna, W.J. Brackenbury, D. Theodorou, M. Koyuturk, H. Kaya, E. Battaloglu, M.T. De Bella, M.J. Slade, R. Tolhurst, C. Palmieri, J. Jiang, D.S. Latchman, R.C. Coombes, M.B. Djamgoz, Voltage-gated sodium channel expression and potentiation of human breast cancer metastasis, Clin. Cancer Res. 11 (2005) 5381–5389.
[4] A.B. Parekh, J.W. Putney Jr., Store-operated calcium channels, Physiol. Rev. 85 (2005) 757–810.
[5] B. Hille (Ed.), Ion Channels of Excitable Membranes, Sinauer, third ed., 2001.
[6] F. Lang, M. Foller, K.S. Lang, P.A. Lang, M. Ritter, E. Gulbins, A. Vereninov, S.M. Huber, Ion channels in cell proliferation and apoptotic cell death, J. Membr. Biol. 205 (2005) 147–157.
[7] M.A. Razik, J.A. Cidlowski, Molecular interplay between ion channels and the regulation of apoptosis, Biol. Res. 35 (2002) 203–207.
[8] D. Haussinger, The role of cellular hydration in the regulation of cell function, Biochem. J. 313 (Pt 3) (1996) 697–710.
[9] F. Lang, G.L. Busch, M. Ritter, H. Volkl, S. Waldegger, E. Gulbins, D. Haussinger, Functional significance of cell volume regulatory mechanisms, Physiol. Rev. 78 (1998) 247–306.
[10] J. Furst, M. Gschwentner, M. Ritter, G. Botta, M. Jakab, M. Mayer, L. Garavaglia, C. Bazzini, S. Rodighiero, G. Meyer, S. Eichmuller, E. Woll, M. Paulmichl, Molecular and functional aspects of anionic channels activated during regulatory volume decrease in mammalian cells, Pflugers Arch. 444 (2002) 1–25.
[11] Y. Okada, T. Shimizu, E. Maeno, S. Tanabe, X. Wang, N. Takahashi, Volume-sensitive chloride channels involved in apoptotic volume decrease and cell death, J. Membr. Biol. 209 (2006) 21–29.
[12] M.R. Shen, T.P. Yang, M.J. Tang, A novel function of BCL-2 overexpression in regulatory volume decrease. Enhancing swelling-activated Ca(2+) entry and Cl(−) channel activity, J. Biol. Chem. 277 (2002) 15592–15599.
[13] Y.M. Shuba, N. Prevarskaya, L. Lemonnier, F. Van Coppenolle, P.G. Kostyuk, B. Mauroy, R. Skryma, Volume-regulated chloride conductance in the LNCaP human prostate cancer cell line, Am. J. Physiol. Cell Physiol. 279 (2000) C1144–C1154.
[14] L. Lemonnier, N. Prevarskaya, Y. Shuba, F. Vanden Abeele, B. Nilius, J. Mazurier, R. Skryma, Ca^{2+} modulation of volume-regulated anion channels: evidence for colocalization with store-operated channels, FASEB J. 16 (2002) 222–224.
[15] F. Vanden Abeele, M. Roudbaraki, Y. Shuba, R. Skryma, N. Prevarskaya, Store-operated Ca^{2+} current in prostate cancer epithelial cells. Role of endogenous Ca^{2+} transporter type 1, J. Biol. Chem. 278 (2003) 15381–15389.
[16] C. Hartzell, I. Putzier, J. Arreola, Calcium-activated chloride channels, Annu. Rev. Physiol. 67 (2005) 719–758.
[17] C. Duran, C.H. Thompson, Q. Xiao, H.C. Hartzell, Chloride channels: often enigmatic, rarely predictable, Annu. Rev. Physiol. 72 (2010) 95–121.
[18] A. Caputo, E. Caci, L. Ferrera, N. Pedemonte, C. Barsanti, E. Sondo, U. Pfeffer, R. Ravazzolo, O. Zegarra-Moran, L.J. Galietta, TMEM16A, a membrane protein associated with calcium-dependent chloride channel activity, Science 322 (2008) 590–594.
[19] Y.D. Yang, H. Cho, J.Y. Koo, M.H. Tak, Y. Cho, W.S. Shim, S.P. Park, J. Lee, B. Lee, B.M. Kim, R. Raouf, Y.K. Shin, U. Oh, TMEM16A confers receptor-activated calcium-dependent chloride conductance, Nature 455 (2008) 1210–1215.
[20] B.C. Schroeder, T. Cheng, Y.N. Jan, L.Y. Jan, Expression cloning of TMEM16A as a calcium-activated chloride channel subunit, Cell 134 (2008) 1019–1029.
[21] M. Katoh, FLJ10261 gene, located within the CCND1-EMS1 locus on human chromosome 11q13, encodes the 8-transmembrane protein homologous to C12orf3, C11orf25 and FLJ34272 gene products, Int. J. Oncol. 22 (2003) 1375–1381.
[22] M. Schwab, Amplification of oncogenes in human cancer cells, Bioessays 20 (1998) 473–479.
[23] J.A. Akervall, Y. Jin, J.P. Wennerberg, U.K. Zatterstrom, E. Kjellen, F. Mertens, R. Willen, N. Mandahl, S. Heim, F. Mitelman, Chromosomal abnormalities involving 11q13 are associated with poor prognosis in patients with squamous cell carcinoma of the head and neck, Cancer 76 (1995) 853–859.

[24] X. Huang, T.E. Godfrey, W.E. Gooding, K.S. McCarty, S.M. Gollin, Comprehensive genome and transcriptome analysis of the 11q13 amplicon in human oral cancer and synteny to the 7F5 amplicon in murine oral carcinoma, Genes Chromosom. Cancer 45 (2006) 1058–1069.
[25] R.B. West, C.L. Corless, X. Chen, B.P. Rubin, S. Subramanian, K. Montgomery, S. Zhu, C.A. Ball, T.O. Nielsen, R. Patel, J.R. Goldblum, P.O. Brown, M.C. Heinrich, M. Van de Rijn, The novel marker, DOG1, is expressed ubiquitously in gastrointestinal stromal tumors irrespective of KIT or PDGFRA mutation status, Am. J. Pathol. 165 (2004) 107–113.
[26] Z. Chen, J. Gu, Immunoglobulin G expression in carcinomas and cancer cell lines, FASEB J. 21 (2007) 2931–2938.
[27] Y. Kanemura, H. Mori, S. Kobayashi, O. Islam, E. Kodama, A. Yamamoto, Y. Nakanishi, N. Arita, M. Yamasaki, H. Kano, M. Hara, J. Miyake, Evaluation of in vitro proliferative activity of human fetal neural stem/progenitor cells using indirect measurements of viable cells based on cellular metabolic activity, J. Neurosci. Res. 69 (2002) 869–879.
[28] X. Zeng, S.C. Sikka, L. Huang, C. Sun, C. Xu, D. Jia, A.B. Abdel-Mageed, J.E. Pottle, J.T. Taylor, M. Li, Novel role for the transient receptor potential channel TRPM2 in prostate cancer cell proliferation, Prostate Cancer Prostatic Dis 13 (2010) 195–201.
[29] L. Shao, Y. Cui, H.Y. Li, Y. Liu, H.S. Zhao, Y. Wang, Y.M. Zhang, K.M. Ng, W.L. Han, D.L. Ma, Q. Ta, CMTM5 exhibits tumor suppressor activities and is frequently silenced by methylation in carcinoma cell lines, Clin. Cancer Res. 13 (2007) 5756–5762.
[30] Y. Wang, H. Zhang, Y.P. Chen, Y.M. Sun, F. Yang, W.H. Yu, J. Liang, L.Y. Sun, X.H. Yang, L. Shi, R.F. Li, Y.Y. Li, Y. Zhang, Q. Li, X. Yi, Y.F. Shang, LSD1 is a subunit of the NuRD complex and targets the metastasis programs in breast cancer, Cell 138 (2009) 660–672.
[31] P.C. Lee, R. Kakadiya, T.L. Su, T.C. Lee, Combination of bifunctional alkylating agent and arsenic trioxide synergistically suppresses the growth of drug-resistant tumor cells, Neoplasia 12 (2010) U372–U376.
[32] S.M. Pulukuri, C.S. Gondi, S.S. Lakka, A. Jutla, N. Estes, M. Gujrati, J.S. Rao, RNA interference-directed knockdown of urokinase plasminogen activator and urokinase plasminogen activator receptor inhibits prostate cancer cell invasion, survival, and tumorigenicity in vivo, J. Biol. Chem. 280 (2005) 36529–36540.
[33] A. Chlenski, K. Nakashiro, K.V. Ketels, G.I. Korovaitseva, R. Oyasu, Androgen receptor expression in androgen-independent prostate cancer cell lines, Prostate 47 (2001) 66–75.
[34] A. van Bokhoven, M. Varella-Garcia, C. Korch, W.U. Johannes, E.E. Smith, H.L. Miller, S.K. Nordeen, G.J. Miller, M.S. Lucia, Molecular characterization of human prostate carcinoma cell lines, Prostate 57 (2003) 205–225.
[35] F. Alimirah, J. Chen, Z. Basrawala, H. Xin, D. Choubey, DU-145 and PC-3 human prostate cancer cell lines express androgen receptor: implications for the androgen receptor functions and regulation, FEBS Lett. 580 (2006) 2294–2300.
[36] K.R. Stone, D.D. Mickey, H. Wunderli, G.H. Mickey, D.F. Paulson, Isolation of a human prostate carcinoma cell line (DU 145), Int. J. Cancer. 21 (1978) 274–281.
[37] C. Ayoub, C. Wasylyk, Y. Li, E. Thomas, L. Marisa, A. Robe, M. Roux, J. Abecassis, A. de Reynies, B. Wasylyk, ANO1 amplification and expression in HNSCC with a high propensity for future distant metastasis and its functions in HNSCC cell lines, Br. J. Cancer 103 (2010) 715–726.
[38] T.K. Klausen, A. Bergdahl, C. Hougaard, P. Christophersen, S.F. Pedersen, E.K. Hoffmann, Cell cycle-dependent activity of the volume- and Ca^{2+}-activated anion currents in Ehrlich lettre ascites cells, J. Cell Physiol. 210 (2007) 831–842.
[39] K. Kunzelmann, Ion channels and cancer, J. Membr. Biol. 205 (2005) 159–173.
[40] J.V. Tapia-Vieyra, J. Mas-Oliva, Apoptosis and cell death channels in prostate cancer, Arch. Med. Res. 32 (2001) 175–185.
[41] S.D. Catz, J.L. Johnson, Transcriptional regulation of bcl-2 by nuclear factor kappa B and its significance in prostate cancer, Oncogene 20 (2001) 7342–7351.
[42] N. Prevarskaya, R. Skryma, G. Bidaux, M. Flourakis, Y. Shuba, Ion channels in death and differentiation of prostate cancer cells, Cell Death Differ. 14 (2007) 1295–1304.
[43] S.L. Zhang, Y. Yu, J. Roos, J.A. Kozak, T.J. Deerinck, M.H. Ellisman, K.A. Stauderman, M.D. Cahalan, STIM1 is a Ca^{2+} sensor that activates CRAC channels and migrates from the Ca^{2+} store to the plasma membrane, Nature 437 (2005) 902–905.